PHYSICAL MECHANISMS ASSOCIATED WITH INITIATION AND PROPAGATION OF KINK-BANDS

R. Gutkin, S. T. Pinho, P. Robinson, P.T. Curtis

The Composites Centre, Department of Aeronautics, Imperial College London
South Kensington, London, SW7 2AZ, England.
r.gutkin07@imperial.ac.uk

ABSTRACT

When compressed in the longitudinal direction, unidirectional Carbon Fibre Reinforced Polymers (CFRP) often fail by kink-band formation. Kink-band initiation and propagation in unidirectional CFRP was studied by in-situ observations under an optical microscope and a Scanning Electron Microscope (SEM). An analytical formulation, based on the experimental evidence, was developed to predict the longitudinal compressive strength and the kink-band geometry as a function of the applied load. The model captures some of the features observed experimentally and predicts longitudinal compressive strengths in the range of values typically measured.

1. INTRODUCTION

Longitudinal compressive strength of unidirectional CFRP is typically half of the tensile strength, which can be a limiting factor for design purposes. The variety and complexity of failure modes which occur during longitudinal compressive failure make it difficult to accurately model this failure process and also to understand how to improve the compressive properties of these materials.

In standard carbon/epoxy systems, a common mode of failure is the formation of kink-bands. As shown in Fig. 1 (a, b), kink-bands in composite materials are regions where fibres have undergone significant rotation over a small distance. In Fig. 1(b), key kink-band parameters are shown: w, the kink-band width; α, the angle of the fibres within the kink-band; β, the kink-band angle.

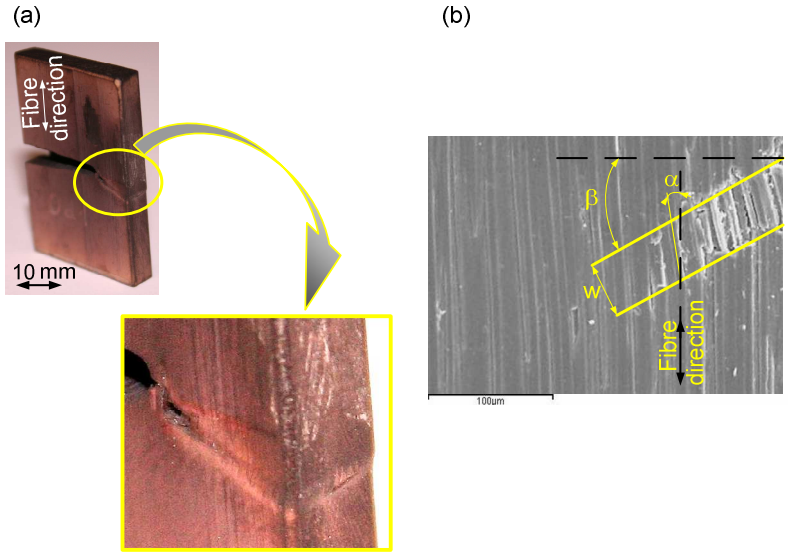

Figure 1: (a) Kink-band in a unidirectional CFRP specimen; (b) Characteristic kink-band parameters.

Analytical models to predict the longitudinal compressive strength of composites failing by kink-band formation have been developed since the early 70's, Argon [1] and Budiansky [2]. In these models, it was assumed that initially misaligned fibres experience additional rotation, due to the compressive loading, until the shear stress in the matrix reaches its yield strength. The corresponding applied stress is then taken as the longitudinal compressive strength of the composite. Budiansky's formulation was later extended by Fleck and Budiansky [3], so that various matrix behaviours and multi-axial loading state could be included (see Fleck [4] for a review).

Hahn [5] and Fleck [6] proposed models to characterise the geometry of kink-bands. Predictions of the kink-band width were achieved by assuming that the width was defined by failure of the fibres.

The present work has focused on an analytical formulation to predict the kink-band width and angle of the fibres within the band. The formulation was based on experimental evidence showing that the kink-band width was defined by broken fibres and by splitting of the fibre/matrix interface.

2. EXPERIMENTAL INVESTIGATION

2.1 Experimental setup

To understand the mechanisms underlying kink-band formation, experiments need to be conducted at the micro-scale of the fibres and matrix. To achieve this, a testing rig was developed to initiate and propagate kink-bands in a controlled way. Once the kink-band was initiated, the testing rig was placed under an optical microscope or in a SEM chamber and the specimens were observed while remaining loaded.
The specimens were 20 mm wide, 20 mm high, 5 mm thick and made of unidirectional CRFP. A 15 mm long notch was cut out to facilitate kink-band formation. The surfaces of the specimens were polished to improve the quality of the pictures.

2.2 Experimental observations

Fig.2 shows a micrograph of a loaded kink-band. Moving along the band from label 1 to 5, the sequence of events leading to kink-band formation can be inferred. In the micrograph labelled 1, the fibres have a pronounced sine-wave shape, but few fibres are broken and the kink-band edges are not fully defined. In micrographs 2 and 3 (left part), the bottom edge of the band is defined with broken fibres. The formation of the top edge is delayed and is fully defined 30 fibre diameters after the bottom edge (see micrograph 4). In micrograph 5, a third edge has formed and the kink-band has a V-shape aspect pointing out the plane of the specimen.

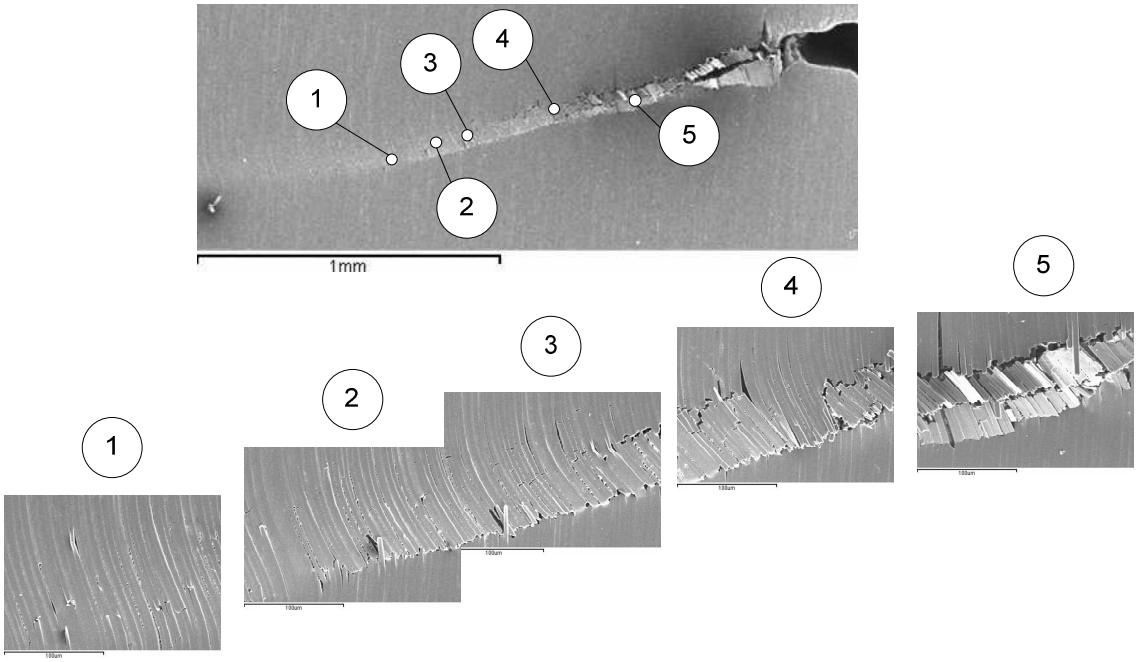

Figure 2: Micrographs at various locations along a loaded kink-band.

Another feature observed in all the micrographs is splitting which runs along the fibre/matrix interface. Fig. 3 shows a close-up view at the bottom edge of the kink-band. The splits S1, S2, S3 are open up to the fibre break. For the split S4, the fibre has not yet failed, but the split is fully open. From Figs. 2 and 3, it can also be seen that the splitting distribution is not uniform along the kink-band: in the micrographs 4 and 5 of Fig. 2, splitting is observed at every fibre/matrix interface while it becomes sparser at micrographs 2 and 3.

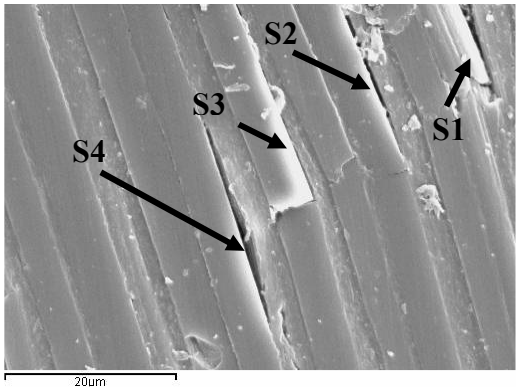

Figure 3: Close-up view of a kink-band edge.

3. ANALYTICAL FORMULATION

3.1 Assumptions

The experimental observations indicate that as the fibres rotate under the compressive load, the fibre/matrix interface fails and the created split remains open under the tensile transverse stress acting within the kink-band. As the compression is increased, the split grows along the fibre direction until the fibres fail by bending.

The present model assumes that kink bands are formed as follows (see Fig. 4): (i) the fibres are locally misaligned, and the misalignment can be represented by a sine shape;

(ii) the matrix is split over the whole misaligned region; (iii) as the composite is loaded in compression, the split region grows if it is energetically favourable for it to do so; and (iv) when the stresses in the fibres reach the corresponding strength, the fibres break and the final geometry of the kink band is defined.

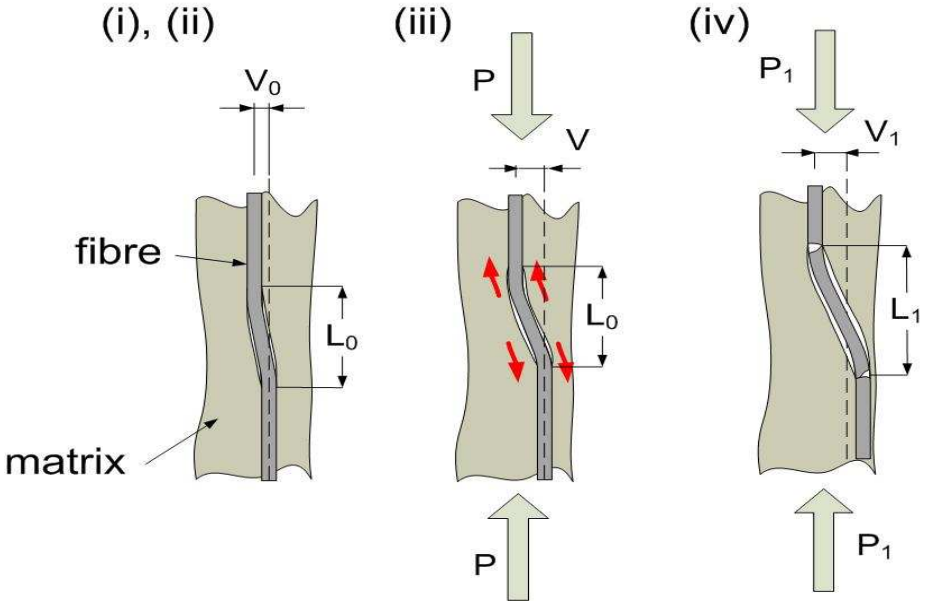

Figure 4: Assumed sequence of events leading to kink-band formation.

Two other important assumptions are that the bending contribution of the matrix can be neglected and that, as the splits along the fibres are open, so no tractions are transmitted from the matrix to the fibre along the split.

3.2 Theory

As mentioned, the present model assumes the kink-band width is defined by the length of the split L at fibre failure. Two equations are needed to define this width: one equation governing the growth of the split as a function of the applied load, and a second equation to define fibre failure load for a split of length L. These equations are derived from the displacement of the fibre found from beam theory.

The initial unloaded fibre is assumed to have a sine-shaped misalignment:

$$v_0(z) = \frac{V_0}{2}\left[1 - \cos\left(\frac{\pi z}{L}\right)\right] \qquad (1)$$

over a length L which corresponds to an existing split, as shown in Fig. 4.

Strictly Eq. (1) should only apply to the initial misalignment i.e. for $L = L_0$. For simplicity, this equation has been assumed to represent the stress-free shape for all split lengths, L. This does introduce an inconsistency concerning the stress-free state of the fibre and the significance of this is to be investigated in further developments of this model. In particular, for small values of L, the rotation of the fibres defined by Eq. (1) is unrealistic, which prevents its application to small lengths L.

At the extremities, where the split stops and the fibre is supported by the matrix, the fibre is assumed to remain straight, giving rise to two end-moments M_1. The fibre is subjected to a compressive end-load P and, since the splits are open, no tractions are transmitted to its lateral surface by the matrix. These conditions are summarised in Figs

5 (a) and (b), where the blue curve with a shape $v_0(z)$ is the initial stress-free configuration and the red curve, with a deflection $u(z)+v_0(z)$, is the deformed configuration.

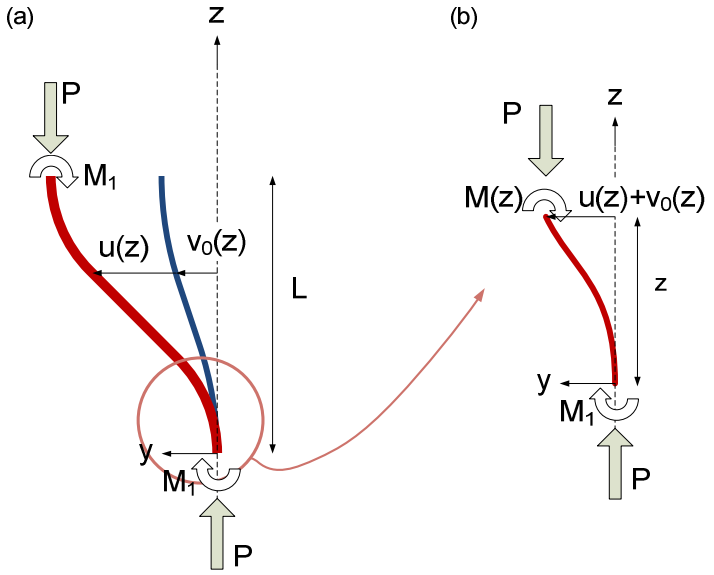

Figure 5: (a) Schematic of the analytical formulation; (b) Free-body diagram.

For this case, the displacement $u(z)$ of the fibre, shown in Fig. 5 (b), can be related to the bending moment *M(z)* using slender beam theory

$$E_f I_f \frac{d^2u}{dz^2}(z) = -M(z), \qquad (2)$$

where E_f is the Young's modulus of the fibre and I_f is the second moment area. The equilibrium of moments for the free-body diagram in Fig. 5(b) results in

$$M(z) = P\big(v_0(z)+u(z)\big) - M_1. \qquad (3)$$

The constant term M_1 in the expression of *M(z)* is unknown. Differentiating Eq. (2) with respect to *z* eliminates this term and with Eq. (3) gives:

$$E_f I_f \frac{d^3u}{dz^3}(z) + P\frac{d}{dz}\big(v_0(z)+u(z)\big) = 0. \qquad (4)$$

With the boundary conditions

$$u(z=0) = 0, \qquad (5)$$

$$\frac{du}{dz}(z=0) = 0, \qquad (6)$$

$$\frac{du}{dz}(z=L) = 0. \qquad (7)$$

The integration of Eq. (4) with Eqs (5-7) gives a displacement

$$u(z) = \frac{V_0/2}{\left(1-\dfrac{P}{P_{cr}}\right)}\frac{P}{P_{cr}}\left(1-\cos\left(\frac{\pi z}{L}\right)\right), \qquad (8)$$

where $P_{cr} = E_f I_f \left(\frac{\pi}{L}\right)^2$.

The split growth along the fibre is governed by two different equations depending on its length: for small split length, a strength criterion is used to predict matrix microcracking; for long split length, the growth is governed by the fracture toughness.

For the strength criterion, matrix cracking is assumed to occur when the shear stress in the matrix is equal to its strength. The shear stress in the matrix is found from the rotation of the compressive stress applied on a frame associated with the misaligned fibres. The rotation of the fibres is derived here under the assumption that the interface is intact. A first shear stress is calculated from stress rotation, in the frame corresponding to the initial misalignment of the fibres

$$\tau_0(z) = \frac{\sigma_c}{2}\sin[2\theta_0(z)], \tag{9}$$

where $\theta_0(z)$ is the initial misalignment angle of the fibres, σ_c is the applied compressive stress, which can be related to the load on the fibre by

$$\sigma_c = \frac{P}{S}\left[V_f + \frac{E_m}{E_f}(1 - V_f)\right]. \tag{10}$$

where E_m is the Young modulus of the matrix, V_f is the fibre volume fraction and S the cross section area of the fibre.

The shear strain in the initial misalignment frame is derived from

$$\gamma_0(z) = \frac{\tau_0}{G_{12}}, \tag{11}$$

where G_{12} is the shear modulus of the composite.

The misaligned angle corresponding to the loaded composite is then calculated as

$$\chi(z) = \gamma_0(z) + \theta_0(z), \tag{12}$$

and the shear stress at the interface between fibre and matrix in the loaded composite becomes

$$\tau(z) = \frac{\sigma_c}{2}\sin[2\chi(z)]. \tag{13}$$

The split is assumed to occur when the average shear stress, $\bar{\tau}$, over a length L reaches the shear strength of the resin

$$\bar{\tau} = \frac{1}{L}\int_0^L \tau(z)dz = S_m. \tag{14}$$

For longer splits, growth occurs when the energy release rate G, for a given length L and a given load P, is equal to the fracture toughness G_c of the interface

$$G = G_c, \tag{15}$$

G is derived for displacement controlled conditions

$$G = -\frac{1}{B}\frac{\partial U}{\partial L}\bigg|_{\delta=\text{constant}}. \tag{16}$$

Where B is the thickness of the fibre δ is the axial displacement due to the bending of the fibre under a given load P. The strain energy, U, is equal to the external work defined by

$$U = \int_0^{\delta} P(\delta) d\delta \,, \tag{17}$$

where δ is

$$\delta = \frac{1}{2}\int_0^L \left(\frac{d}{dz}\left(u(z) + v_0(z)\right)\right)^2 dz - \frac{1}{2}\int_0^L \left(\frac{dv_0(z)}{dz}\right)^2 dz \tag{18}$$

and $P(\delta)$ is found from inverting Eq. (14).

Solving Eqs (14) or (15) gives the split length L for a given applied load P, which was one of the objectives identified earlier.

The other objective is to find the load at fibre failure for a given split length L. Fibre failure is assumed to occur when the maximum compressive stress of the fibre is equal to its strength X_{fc}

$$E_f \frac{d}{2}\frac{d^2u}{dz^2}(L) - \frac{P}{S} = -X_{fc} \,, \tag{19}$$

where d is the radius of the fibre.

The two unknowns P and L can be found by solving Eqs (14) or (15) and (19). The length L of the split is then assumed to be the kink-band width w.

4. RESULTS

4.1 Benchmark results

In the present section, the predictions from Eqs (14) or (15) and (19) are presented for material properties corresponding to IM7-8551-7 carbon/epoxy system, listed in Table 1.

Table 1. Material data.

V_f	E_f (GPa)	d (μm)	X_{fc} (MPa)	E_m (MPa)	S_m (MPa)	G_{12} (MPa)	X_c (MPa)	G_c (kJ/m^2)
0.6	273	7	3200	4200	60	5600	1590	0.4

Fig. 6 shows the plots corresponding to Eqs (14) and (15), labelled interface failure, and Eq. (19), labelled fibre failure. The vertical axis represents the compressive stress applied on the composite, σ_c, the horizontal axis represents a non-dimensionalised kink-band width w/d. The intersection of the curve corresponding to strength-controlled matrix failure with the curve corresponding to fibre failure indicates the length of the split at fibre failure. The curve corresponding to the toughness-controlled matrix failure is found not to influence failure in this case. However, it should be noted that Eq. (15) assumes slender beam theory, which is not valid for small lengths L, and this might be influencing the results.

The first part of the curve for interface failure, indicated by the dashed line in Fig. 6, is not predicted by the model, due to the restricted applicability of Eq. (1), as discussed previously.

The initial misalignment is a material input, a priori unknown. In this section, the magnitude of the initial misalignment (V_0) has been chosen so that the predicted compressive strength matches the experimental one.

In Fig. 6, the initial misalignment is set to $V_0 = 4.10^{-4}$ μm and the compressive strength, which corresponds to σ_c at the point of intersection, is 1575 MPa. At fibre failure, the kink-band width is found to be w/d = 1.8 fibre diameters. The angle of the fibre within

the band at fibre failure, found from the derivative of the displacement, evaluated at fibre mid-length, for $L = w$, is $\alpha = 4.14°$ and the initial misalignment angle is back-calculated from Eq. (1) as $\theta_0 = 2°$.
These results can be compared to Fig. 2 (stage 1), where $w/d = 12$ fibre diameters and $\alpha \approx 20°$.

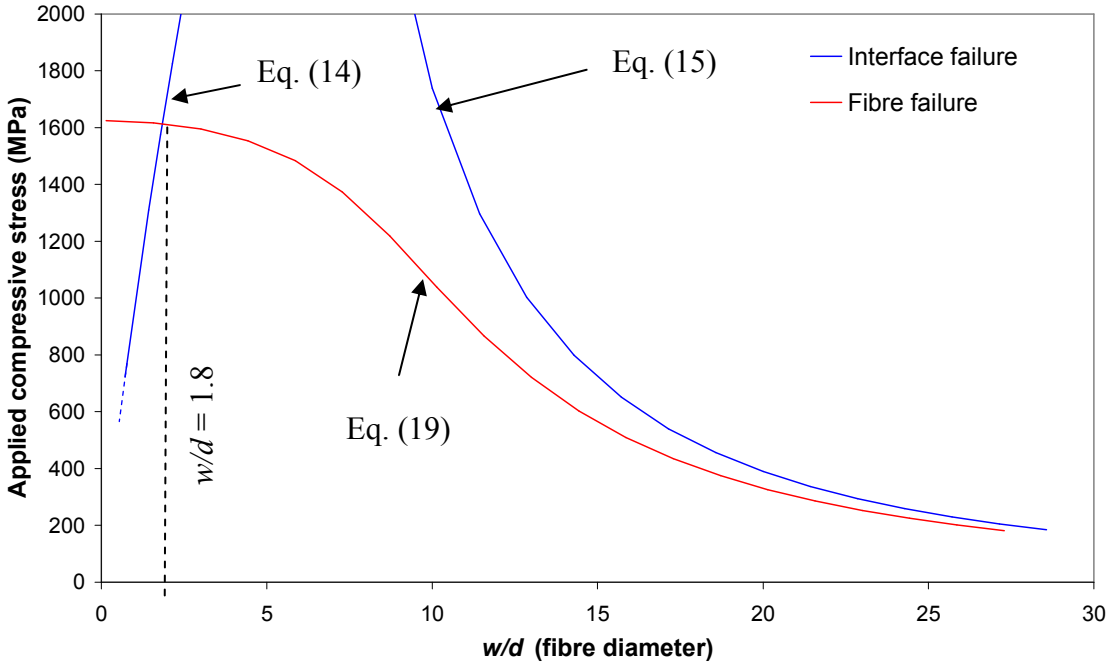

Figure 6: Kink-band width prediction for $V_0 = 4.10^{-4}$ µm.

5. DISCUSSION

From Fig. 6, the model predicts some matrix cracking before the peak load. This is consistent with nonlinearities which have been experimentally observed by Moran et al. [7]. However, it should be noted that the present model cannot predict the stress corresponding to the onset of these nonlinearities. This is due to the limitation of Eq. (1) discussed previously.
For small magnitude of the initial misalignment, Fig. 6, a split is predicted to grow along the fibre up to a length $w/d = 1.8$ fibre diameters. At this point, fibre failure occurs and the composite reaches its compressive strength. The value of the kink-band width w and angle of the fibres within the kink-band α are smaller than those observed experimentally, but the initial misalignment angle predictions compare well with typical values measured for IM7-8551-7 carbon-epoxy composites.
The sequence of events, during kink-band formation, predicted by the model, and the assumptions underlying it, is that matrix cracking occurs first, eventually fibres failure.

6. CONCLUSION

The experimental results presented showed that significant splitting takes place at the fibre/matrix interface within the kink-band. The edges of the kink-band were defined by broken fibres.

The analytical formulation, based on the experimental findings, captured some trends of the process involved in kink-band formation. Other parameters related to the formation of the kink-band were not predicted accurately.
Further work is needed to resolve some inconsistencies related to the assumed initial shape of the fibre and to improve the predictions in terms of kink-band width and angle of the fibres within the kink-band.

ACKNOWLEDGEMENTS

The funding of this research from the Engineering and Physical Sciences Research Council and the Ministry of Defence under the project EP/E0Z3169/1 is gratefully acknowledged. Miss Soraia Pimenta and Mr Will Francis are also acknowledged for working on the experiments as part of their final year projects at the Department of Aeronautics at Imperial College London.

REFERENCES

1- Argon A., "Fracture of composites"*, Treatise on material science and technology*, 1972;1:79-114.
2- Budiansky B., "Micromechanics", *Computers & Structures,* 1983;16:3-12.
3- Budiansky B., Fleck N., "Compressive failure of fibre composites", *Journal of the Mechanics and Physics of Solids,* 1993;41:183-211.
4- Fleck N., "Compressive failure of fiber composites", *Advances in applied mechanics,* 1997;33:43-117.
5- Hahn H.T., Williams, J.G., "Compressive failure mechanisms in unidirectional composites", *Composite materials: Testing and design (Seventh Conference), ASTM STP 893*,1986;115-139.
6- Fleck N.A., Deng L., Budiansky B., "Prediction of kink width in compressed fiber composites", *Journal of Applied Mechanics*, 1995;62:329-337.
7- Moran P.M., Liu X.H., Shih C.F., "Kink band formation and band broadening in fiber composites under compressive loading", *Acta metallugirca materialla,* 1995;43:2943-2958.